Application of a Finite Element Algorithm to the Solution of Steady Transonic Euler Equations

H. U. Akay* and A. Ecer†
Purdue University, Indianapolis, Indiana

A finite element algorithm has been developed for the solution of two-dimensional, steady Euler equations. Through a Clebsch-type transformation for the velocity vector, the conservation of mass equation with one primary variable is solved together with two additional equations for the convection of two new variables. For isentropic and irrotational flows, the procedure automatically reduces to the solution of the potential equation expressed in terms of the velocity potential function only. In this paper, the accuracy and the efficiency of the developed scheme are discussed in detail. The second-order accuracy attained in the analysis of the convection of the vorticity is demonstrated. The efficient treatment of the rotational and irrotational flow subregions are presented. The accuracy of the numerical scheme and its convergence characteristics are demonstrated for a sample problem.

I. Introduction

THE numerical solution of Euler equations for steady transonic flows is often based on the asymptotic solutions of the unsteady equations which are expressed in terms of the primitive variables ρ, u, v, and p.[1-3] Efficient schemes for obtaining fast convergence to a steady state have been investigated by several researchers in recent years. The main difficulties in the solution of these equations arise due to the mixed elliptic-hyperbolic nature of these equations and the requirements for their stable integration in time.[4]

A different approach to solving the Euler equations is to cast them into a new set, using a transformation of variables, and to solve the new set of equations in terms of the transformed variables. A classical example of this approach is the use of streamfunctions and vorticities as the basic variables. The present procedure is based on a similar approach. The velocities are expressed in terms of a new set of variables using a Clebsch-type transformation.[5]

The derivation of the related governing equations was presented previously in Ref. 6. In the present paper, further details of the formulation are given and some of the fundamental characteristics of the solutions of Euler equations are investigated using a transonic flow problem in a channel as the test case. The finite element method is used in the analysis, which allow the application of a Ritz- or Galerkin-type procedure in constructing the discretized equations for irregular computational grids and general boundary conditions in a convenient manner.

II. Euler Equations

The derivation of the Euler equations using a variational formulation and Clebsch transformation was discussed for general flows in Ref. 6. In this paper, the discussions are restricted to steady, two-dimensional transonic flows only. In terms of the primitive variables, the governing equations are

$$(\rho u)_{,x}+(\rho v)_{,y}=0 \tag{1}$$

$$(\rho u^2+p)_{,x}+(\rho uv)_{,y}=0 \tag{2}$$

$$(\rho uv)_{,x}+(\rho v^2+p)_{,y}=0 \tag{3}$$

where ρ, p, u, v are density, pressure, and velocity components, respectively, and the comma denotes partial differentiation. Equation (1) is the conservation of mass and Eqs. (2) and (3) are the equations of motion in x and y directions, respectively. Since the flow is steady, the total enthalpy

$$H_0=H+\frac{1}{2}(u^2+v^2)=\frac{\gamma}{\gamma-1}\frac{p}{\rho}+\frac{1}{2}(u^2+v^2) \tag{4}$$

is constant along a streamline, and H is the specific enthalpy and γ the ratio of specific heats. This provides the necessary relationship between ρ and p so that Eqs. (1-3) can be solved for ρ, u, and v.

It is also possible to reformulate the above problem when the vorticity

$$\zeta=v_{,x}-u_{,y} \tag{5}$$

is introduced as a new variable. By considering the dynamic motion of a rotating fluid particle in streamline coordinates, one can replace Eqs. (2) and (3) with the Crocco relationship[7]

$$\zeta=1/q(TS_{,n}-H_{0,n}) \tag{6}$$

where

$$q=(u^2+v^2)^{1/2} \tag{7}$$

is the flow speed, S the entropy, T the temperature, and n the direction normal to the streamlines. Using the gas law $p=\rho RT$, Eq. (6) can further be expressed in the form

$$\frac{\zeta}{p}=\frac{1}{q}\left(\frac{1}{\rho R}S_{,n}-\frac{1}{p}H_{0,n}\right) \tag{8}$$

which is constant along a streamline,[8] or,

$$\boldsymbol{u}\cdot\nabla(\zeta/p)=0 \text{ everywhere} \tag{9}$$

where $\boldsymbol{u}$ is the velocity vector and ∇ is the gradient operator. Therefore, Eqs. (5) and (9) together with the conservation of mass in Eq. (1) provide a new set of governing equations for inviscid rotational flows.

By introducing a streamfunction which satisfies Eq. (1) automatically, Emmons[9] and more recently Hafez and Lovell[10] have solved Eqs. (5) and (6) iteratively with the streamfunction as the only primary variable.

III. Variational Statement

The present formulation starts with a variational theorem which states that the stationary values of the following

Presented as Paper 82-0970 at the AIAA/ASME Third Joint Thermophysics, Fluid, Plasma and Heat Transfer Conference, St. Louis, Mo., June 7-11, 1982; submitted June 11, 1982; revision received Jan. 25, 1983.

*Associate Professor, School of Engineering and Technology. Member AIAA.

†Professor, School of Engineering and Technology. Member AIAA.

functional provides the Eulerian equations of motion for two-dimensional, steady transonic flows.

$$\pi+\int_\Omega \{L+\phi[\nabla\cdot(\rho u)]+\beta_i[\nabla\cdot(\rho\alpha_i u)]\}\,d\Omega \tag{10}$$

where

$$L=\tfrac{1}{2}\rho(u^2+v^2)-\rho E \tag{11}$$

is the Lagrangian density, $E=p/[\rho(\gamma-1)]$ the internal energy per unit mass, Ω the Eulerian region, α_i $(i=1,2)$ are the material coordinates, ϕ and β_i the Lagrangian multipliers.

As can be seen from the above variational statement, the Lagrangian, which involves both the kinetic energy and the internal energy of the fluid particles, is augmented by the conservation of material coordinates and the conservation of mass equations as constraints. The introduction of the conservation of material coordinates is essential in the formulation in order to preserve the identity of the particles which occupy the Eulerian region Ω. Although, two material coordinates are needed to define the position of a particle in two-dimensional steady flows, only one curvilinear material coordinate normal to the flow direction, say $\alpha_1=\alpha$, is sufficient to describe its identity throughout the motion. Therefore, in Eq. (10), the conservation equation for only α_1 is to be used as a constraint.

It can be shown further that the above variational functional is equivalent to the Bateman functional, which, with nonhomogeneous boundary conditions, can simply be expressed as[5,6]

$$\pi+\int_\Omega p\,d\Omega+\int_{\Gamma_{2\phi}} f_\phi\phi\,d\Gamma+\int_{\Gamma_{2\beta}} f_\beta\beta\,d\Gamma \tag{12}$$

where f_ϕ and f_β are the known boundary fluxes which are calculated from

$$f_\phi=\rho u\cdot n \text{ on boundary } \Gamma_{2\phi} \tag{13}$$

$$f_\beta=\rho\alpha u\cdot n \text{ on boundary } \Gamma_{2\beta} \tag{14}$$

respectively.

By using the equation of state

$$p=\kappa\rho^\gamma e^{(\gamma-1)S/R} \tag{15}$$

and the total enthalpy in Eq. (4), the variational functional reduces to

$$\pi=\int_\Omega c\left[H_0-\frac{1}{2}u_iu_i\right]^\theta e^{-S/R}\,d\Omega+\int_{\Gamma_{2\phi}} f_\phi\phi\,d\Gamma+\int_{\Gamma_{2\beta}} f_\beta\beta\,d\Gamma \tag{16}$$

where

$$\theta=\gamma/(\gamma-1),\quad c=\kappa(\kappa\theta)^{-\theta},\quad \kappa=\text{const} \tag{17}$$

The unknowns in the above expression are u, v, S, ϕ, α, and β. However, if one employs a Clebsch transformation for the velocity vector in the following form

$$u=\nabla\phi+\alpha\nabla\beta \tag{18}$$

and considers that, for steady flows, the entropy and the total enthalpy can be determined from the following relations:

$$S=S_0(\alpha) \text{ and } H_0=H_0(\alpha) \tag{19}$$

where S_0 is the initial entropy distribution, then the stationary values of the variational functional in Eq. (16) produces the following set of equations:

$$\nabla\cdot(\rho u)=0 \tag{20}$$

$$\rho u\cdot\nabla\beta=-(p/R)S_{,\alpha}+\rho H_{0,\alpha} \tag{21}$$

$$\nabla\cdot(\rho\alpha u)=0 \tag{22}$$

In the analysis of steady transonic flows, the flow can be assumed to be isentropic, isoenergetic, and irrotational until shock waves interfere. After the shock the flow will still remain isoenergetic, although no longer isentropic and irrotational. The entropy distribution after the shock, however, can be determined in terms of material coordinate α by using the Rankine-Hugoniot shock-jump conditions.[6] Equations (20-22) can also be applied to more general rotational flows once the total enthalpy distribution $H_0(\alpha)$ due to rotationality, is specified at the far field upstream.

The primary variables of this new set of Euler equations are ϕ, α, and β. Therefore, rather than solving Eqs. (1-3) for ρ, u, and v, we need to determine ϕ, α, and β from Eqs. (20-22). The physical variables ρ, p as well as the kinematic variables u, v, ζ are the derived quantities of these equations. They are derived from the material coordinate α which remains constant along a streamline, and from the Lagrange multipliers ϕ and β which enforce the conservation of mass and the conservation of material coordinates, respectively.

Using Eqs. (5) and (18), the vorticity can be expressed in terms of these variables as

$$\zeta=\alpha_{,x}\beta_{,y}-\alpha_{,y}\beta_{,x}=-\alpha_{,n}\beta_{,s} \tag{23}$$

where s denotes the local streamline direction. It is interesting to note that if β is eliminated from Eqs. (21) and (23), the vorticity becomes

$$\zeta=1/q(TS_{,\alpha}-H_{0,\alpha})\alpha_{,n} \tag{24}$$

which is precisely the Crocco relation given by Eq. (6). Therefore, Eq. (21) of the new formulation is equivalent to the momentum equations (2) and (3).

In the case of isentropic flows, β becomes a constant from Eq. (21), and the Clebsch representation in Eq. (18) produces the potential flow formulation

$$u=\nabla\phi \tag{25}$$

In this case, the so-called velocity potential function is the Lagrange multiplier for the conservation of mass which remains as the only equation to be solved. An important convenience with the present formulation is the link between isentropic and nonisentropic flow regions. For the isentropic flow regions, β is set to a constant and only one variable ϕ is calculated from Eq. (20). For nonisentropic flow regions all three variables, ϕ, α, and β, must be calculated from Eqs. (20-22).

IV. Solution of Equations

Instead of solving the two convective equations (21) and (22) directly, it is more convenient to transform each into a second-order differential equation by premultiplying with the convective operator $\rho u\cdot\nabla$. Therefore, assuming that $H_0(\alpha)$ is constant, Eqs. (20-22) become

$$\nabla\cdot(\rho\nabla\phi)+\nabla\cdot(\rho\alpha\nabla\beta)=0 \tag{26}$$

$$\rho u\cdot\nabla\left(\frac{1}{T}u\cdot\nabla\beta\right)=0 \tag{27}$$

$$\rho u\cdot\nabla(\rho u\cdot\nabla\alpha)=0 \tag{28}$$

Then the flux-type boundary conditions specifying the flux of mass and entropy at the boundaries in this case can be written as

$$\rho u\cdot n=f_\phi \text{ on } \Gamma_{2\phi} \tag{29}$$

for Eq. (26), and

$$-S,_{\alpha}(\rho \boldsymbol{u}\cdot\boldsymbol{n}) = f_{\alpha} \text{ on } \Gamma_{2\alpha} \tag{30}$$

for Eq. (27).

Finite element discretizations of Eqs. (26-28) are straightforward. When Galerkin-type approximations are used, the following nonlinear equations in the discrete form are obtained.

$$\boldsymbol{K}_{\phi\phi}\boldsymbol{\phi} + \boldsymbol{K}_{\phi\beta}\boldsymbol{\beta} = \boldsymbol{f}_{\phi} \tag{31}$$

$$\boldsymbol{K}_{\alpha\beta}\boldsymbol{\beta} = \boldsymbol{f}_{\alpha} \tag{32}$$

$$\boldsymbol{K}_{\beta\alpha}\boldsymbol{\alpha} = \boldsymbol{0} \tag{33}$$

where $\boldsymbol{K}_{ij}$ are the symmetric nonlinear coefficient matrices. Explicit forms of the coefficient matrices may be found in Ref. 6.

For the numerical solution of Eqs. (31-33) the following pseudo-time-dependent scheme is employed:

$$\boldsymbol{K}^{n}_{\phi\phi}\dot{\boldsymbol{\phi}}^{n} + \boldsymbol{K}^{n}_{\phi\beta}\dot{\boldsymbol{\beta}}^{n} = \boldsymbol{f}^{n}_{\phi} - \boldsymbol{K}^{n}_{\phi\phi}\boldsymbol{\phi}^{n} - \boldsymbol{K}^{n}_{\phi\beta}\boldsymbol{\beta}^{n} = \boldsymbol{R}^{n}_{\phi} \tag{34}$$

$$\boldsymbol{K}^{n}_{\alpha\beta}\dot{\boldsymbol{\beta}}^{n} = \boldsymbol{f}^{n}_{\alpha} - \boldsymbol{K}^{n}_{\alpha\beta}\boldsymbol{\beta}^{n} = \boldsymbol{R}^{n}_{\alpha} \tag{35}$$

$$\boldsymbol{K}^{n}_{\beta\alpha}\dot{\boldsymbol{\alpha}}^{n} = -\boldsymbol{K}^{n}_{\beta\alpha}\boldsymbol{\alpha}^{n} = \boldsymbol{R}^{n}_{\beta} \tag{36}$$

with

$$\boldsymbol{\phi}^{n+1} = \omega\dot{\boldsymbol{\phi}}^{n} + \boldsymbol{\phi}^{n} \text{ etc.} \tag{37}$$

where n is the pseudo-time (iteration) step, ω the relaxation factor, and $\boldsymbol{R}^{n}_{i}$ the residual vectors. When Eq. (35) is solved before Eq. (34), then Eqs. (34-36) can be solved as an uncoupled set of equations for ϕ, α, and β. The above set of equations is integrated until a steady state is reached, i.e., when the residuals approach zero.

V. Discussion of Results

A transonic flow through a parallel channel with a 10%-thick circular bump and an upstream Mach number of 0.675 was analyzed here with the developed numerical procedure. This problem was previously tested by Ni,[2] who has developed a multigrid scheme for solving the full Euler equations with the primitive variables ρ, u, v. The computational grid shown in Fig. 1, which has a total of $60 \times 12 = 720$ elements, was employed as the basic grid for this analysis. As will be presented subsequently, some modified versions of this grid were also employed to investigate the sensitivity of the results to the local changes in the grid. The obtained Mach number distribution over the bump surface is compared in Fig. 2 with that of Ref. 2. As can be observed, there is a very close agreement between the solutions of the two methods. The resulting Mach contours in the channel are as shown in Fig. 3, where the effect of rotationality on the Mach contours past the shock is apparent. Contours for material coordinate α are given in Fig. 4. Further characteristics of the developed computational method are discussed next.

Convergence Characteristics

Equations (26-28) imply that the solutions of full Euler equations are required only for the subsonic flow region past the shock, since everywhere else the flow is irrotational and isentropic. Also, because for this particular problem the shock is only moderately strong even in the irrotational case, we expect the Euler solution to be reasonably close to the potential solution. Therefore, rather than solving the full Euler equations with all three variables (ϕ, α, and β) directly, the flow was first assumed to be isentropic everywhere, and an irrotational solution was first obtained by solving Eq. (26) for

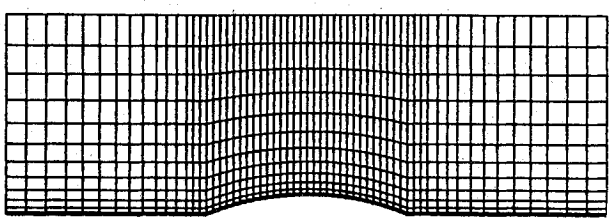

Fig. 1 Basic computational grid for the channel (grid A).

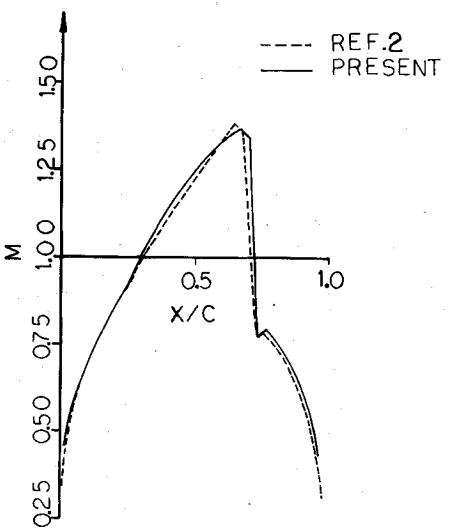

Fig. 2 Rotational flow, Mach distribution over the bump surface.

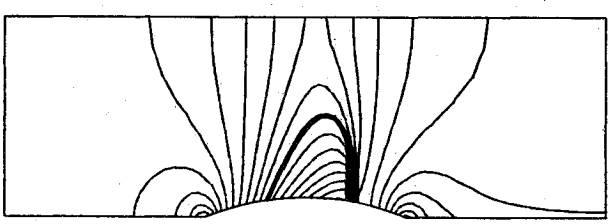

Fig. 3 Mach contours for the rotational flow ($\Delta M = 0.05$).

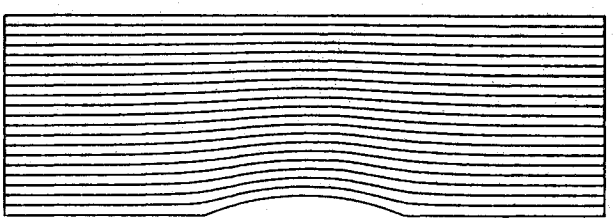

Fig. 4 Contours for material coordinate α ($\Delta\alpha = 0.05$, $\alpha_{min} = 0$, $\alpha_{max} = 1.0$).

ϕ only. Mach contours for this case are as shown in Fig. 5. Then, starting with this isentropic solution as an initial guess, full Euler equations were solved.

The rate of convergence of the solutions can be observed from Fig. 6, in which the entire history of the residuals is plotted.

For the isentropic solution first a shock capturing scheme was applied for approximately 90 iteration steps with a relaxation parameter of $\omega = 0.7$. Then, in order to check for correctness of the shock location, a shock fitting[11] was applied for approximately 40 more iterations until the shock position was stabilized at two elements downstream of the initial location predicted by the capturing scheme. Following this, a switch to capturing was made until the maximum

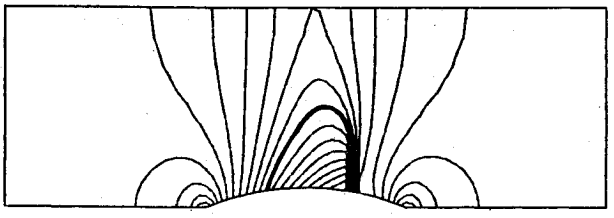

Fig. 5 Mach contours for the irrotational flow ($\Delta M = 0.05$).

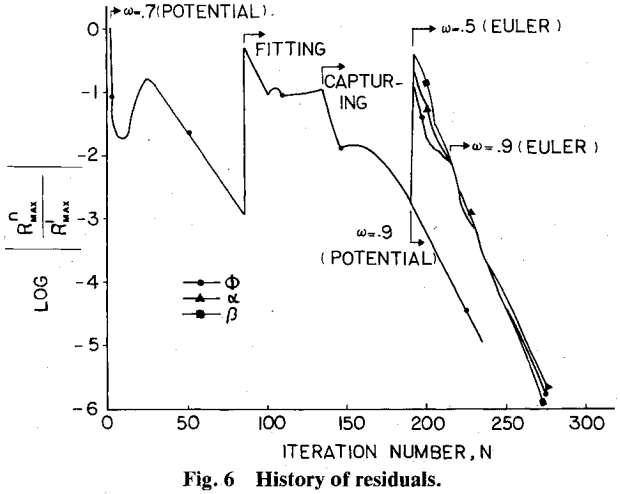

Fig. 6 History of residuals.

residual in ϕ was dropped down to 10^{-3} at about iteration step 190. To further decrease the residuals, the shock capturing solution was continued with a relaxation parameter of 0.9 until the maximum residual was lowered to approximately 10^{-5} at iteration step 240.

For the Euler equations, the reasonably converged solution of the potential solution at iteration step 190 was used as an initial guess. Since the entropy flux defined in Eq. (30) was applied impulsively at the boundary, a lower relaxation parameter of $\omega = 0.5$ was employed for the first 30 steps in order to gradually integrate the initial transient behavior. The relaxation parameter was then increased to $\omega = 0.9$ until the maximum residuals were reduced to 10^{-6} in a total of 85 iterations after the potential solution. During the Euler solutions, β values were specified to be constant over the isentropic flow regions, thus Eq. (27) was solved only in the nonisentropic region.

As can be seen from the residual history curves, the convergence rate of the direct solver employed in this analysis is quite high. In fact, the number of iteration steps for convergence is largely determined by the effort in locating the correct position of the shock by shock fitting and shock capturing schemes in the potential solution, as discussed in Ref. 11. In general, since the isentropic shock is stronger, the shock obtained from the potential solution develops further downstream of the shock from the Euler solution. However, the shock can move upstream automatically in a shock capturing scheme when such a case develops.

The above test case illustrates that one can obtain the same rate of convergence for α and β variables as that obtained for ϕ. This can be explained in terms of the nonlinearity of the equations. Since the main coupling in the equations is through the density ρ, the Lagrange multiplier for the conservation of mass remains the dominant variable in determining the convergence. At least for the problems with moderate shocks, the preceding results suggest that the same rate of convergence of a particular potential flow scheme can be expected from the present Euler formulation. The convergence characteristics of the isentropic flow equations were discussed in Ref. 11. It was shown that the preceding iterative scheme is convergent for

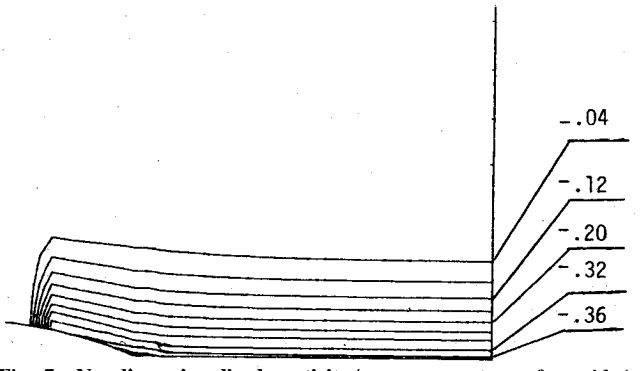

Fig. 7 Nondimensionalized vorticity/pressure contours for grid A ($\Delta\xi = 0.04$).

subsonic flow regions with the rate

$$r = \Delta q_e^{n+1} / \Delta q_e^n = \exp[\omega(M_e^2 - 1)] \tag{38}$$

where Δq_e^n is the error in the speed of element e at time step n, and M_e is the average Mach number for the element.

The extension of the same analysis to the iterative solution of Euler equations can be developed in the following manner: Dropping the subscript e denoting an element, a simple one-dimensional form of the equations ($\alpha = \text{const}$) is considered for a single element by taking $\gamma = 2$ as follows:

$$[H_0^2 - (q^n)^2] N_{,x} N_{,x}^T (\bar{\phi}^{n+1} + \alpha \bar{\beta}^{n+1}) = 0 \tag{39}$$

$$(q^n)^2 N_{,x} N_{,x}^T \bar{\beta}^{n+1} = 0 \tag{40}$$

where N is the vector form of the element shape functions.[11] After assuming

$$\bar{\phi}^{n+1} = \phi + \Delta\phi^{n+1}, \quad |\phi_{,x}| \gg |\Delta\phi_{,x}^{n+1}| \tag{41}$$

$$\bar{\beta}^{n+1} = \beta + \Delta\beta^{n+1}, \quad |\beta_{,x}| \gg |\Delta\beta_{,x}^{n+1}| \tag{42}$$

where ϕ and β are the steady-state values, one can obtain

$$\Delta\bar{\phi}_{,x}^{n+1} + \alpha\Delta\bar{\beta}_{,x}^{n+1} = M^2[\Delta\phi_{,x}^n + \alpha\Delta\beta_{,x}^n] \tag{43}$$

$$\alpha\Delta\bar{\beta}_{,x}^{n+1} = -\frac{|\alpha\beta_{,x}|}{|\phi_{,x} + \alpha\beta_{,x}|}[\Delta\phi_{,x}^n + \alpha\Delta\beta_{,x}^n] \tag{44}$$

The eigenvalues of these systems of equations provide the same convergence rate for ϕ and β as given in Eq. (38). This behavior describes that which was observed in the numerical integration of Euler equations in Fig. 6. Although, for this particular example, the vorticity level is rather low, the numerical results show that once the solution is close to the steady-state solution, the same convergence rate is observed for the isentropic, potential equation. The advantage of the numerical method in terms of efficiency is obvious for the sample problem. Only the velocity potential is calculated for the first part of the analysis. Three variables are calculated only for the nonisentropic flow regions of the flow following the potential solution. It should finally be emphasized that the three variables ϕ, α, and β are calculated independently from Eqs. (34-36), respectively.

Accuracy of the Solutions

The second important consideration in the solution of Euler equations is the accuracy of the obtained numerical results. The same case will be employed again to illustrate the basic problems related to the accuracy. One of the important features of the obtained numerical solution can be observed from the Clebsch presentation of velocities in Eq. (18). This equation suggests that for accurate calculation of velocities at

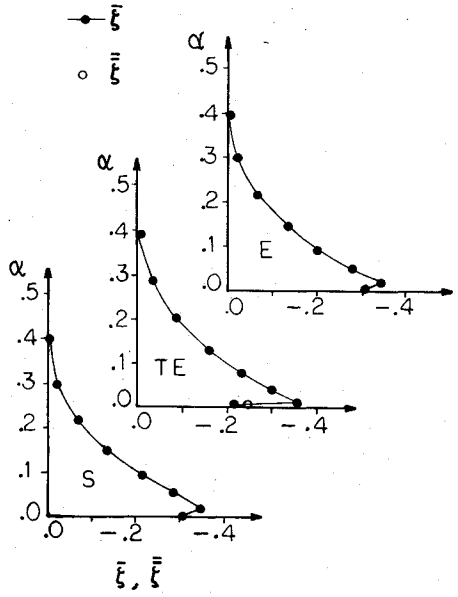

Fig. 8 Nondimensionalized vorticity/pressure profiles for grid A (S, immediately past the shock; TE, trailing edge; E, exit).

least second-order accurate solutions of ϕ and β are required. This is also correct for the calculation of vorticity from Eq. (23). Contours for nondimensionalized vorticity/pressure values for the same problem are plotted in Fig. 7. A check to be employed for the accuracy of the solutions is to calcualte the vorticity from two different relationships: one from Eq. (23) and the other from Crocco's relationship in Eq. (24). If the vorticity is calculated accurately, the vorticity corresponding to the entropy distribution, in Eq. (24), should match the solution calculated from the kinematics of the solution in Eq. (23). For this purpose, two separate non-dimensional vorticity/pressure values are defined as follows.

$$\bar{\zeta}=\frac{\zeta C/a_0}{p/p_0}=-\frac{\alpha_{,n}\beta_{,s}C/a_0}{p/p_0} \tag{45}$$

and

$$\bar{\bar{\zeta}}=\frac{\zeta C/a_0}{p/p_0}=\frac{S_{,n}C/a_0}{\rho qR/p_0} \tag{46}$$

where C is the chord length, a_0 and p_0 are stagnation speed of sound and pressure, respectively.

The profiles of these two variables at selected cross sections are plotted in Fig. 8. As can be seen from these results, the solution is extremely accurate except near the channel walls.

The inaccuracy of the solution at the solid boundaries is due to the singularities developing at these boundaries. As can be seen from Fig. 8, a singularity occurs for vorticity at the trailing edge of the bump. This is due to the calculation of the vorticity from Eq. (23). At any discontinuity on the wall, the vorticities calculated from Eq. (23) approach zero. A different type of singularity can be expected as the velocity approaches zero at the stagnation point and creates a singularity in the solution of Eq. (27). However, for all test problems no numerical difficulty was observed due to this singularity which would tend to cause vorticities to blow up at the stagnation point. Instead, low vorticity values were calculated from Eq. (23).

A similar singularity in vorticity arises at the junction of the shock and the wall boundary. The smooth surface streamline prevents any change in the flow angle across the shock, thus enforcing the shock to be normal at the wall.[9] Therefore, specification of a smooth streamline across the shock again tends to make the vorticity approach zero at the wall boundary.

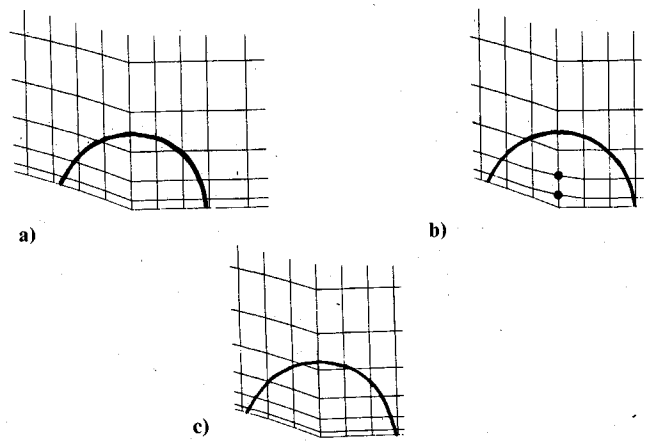

Fig. 9 Grid modifications near the rear stagnation point. a) Basic computational grid (grid A). b) Grid B. c) Grid C.

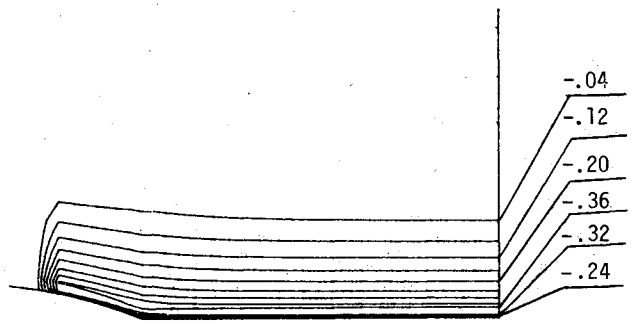

Fig. 10 Nondimensionalized vorticity/pressure contours for grid B ($\Delta\bar{\zeta}=0.04$).

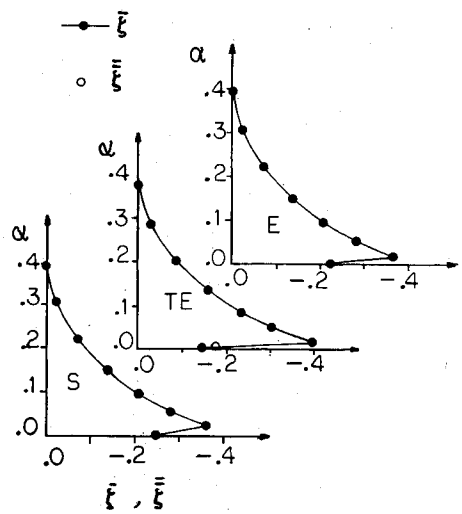

Fig. 11 Nondimensionalized vorticity/pressure profiles for grid B.

Both of these singularities can be described by the following vorticity equation expressed in intrinsic coordinates[8]:

$$\zeta=-\partial q/\partial n+\kappa q \tag{47}$$

where n is the direction normal to the streamline and κ is the curvature of the streamline. At the trailing edge of the bump, the curvature of the streamline becomes discontinuous.[12] On the other hand, across the shock, the vorticity ζ has a jump while the curvature κ is continuous.[9] It should also be remembered that any error introduced at a point will be convected along the particular streamline as defined in Eqs. (27) and (28).

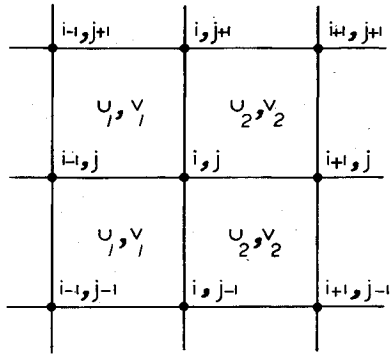

Fig. 12 A uniform finite element model.

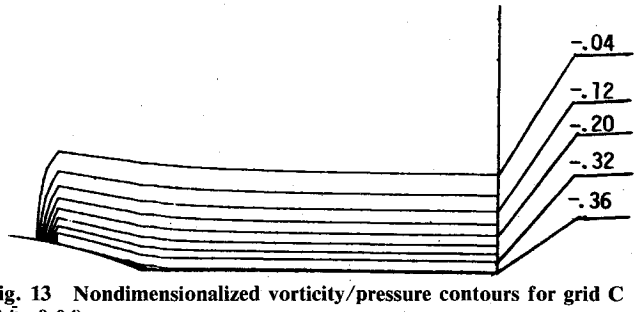

Fig. 13 Nondimensionalized vorticity/pressure contours for grid C ($\Delta\bar{\xi}=0.04$).

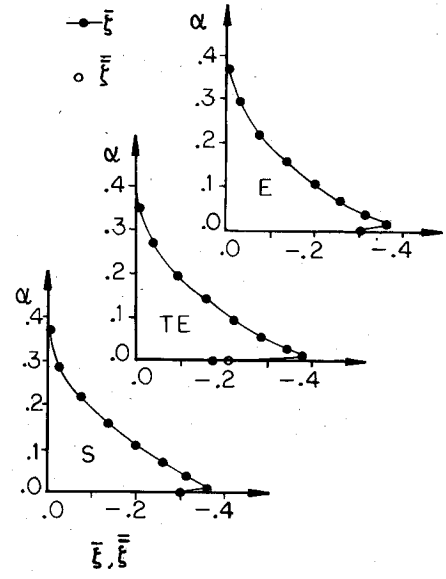

Fig. 14 Nondimensionalized vorticity/pressure profiles for grid C.

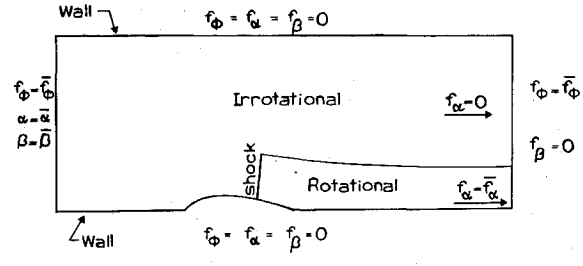

Fig. 15 Boundary conditions.

To illustrate some of the concepts discussed above, some local changes were made in the computational grid shown in Fig. 1. Only the position of two nodes closest to the rear stagnation point were changed as shown in Fig. 9b.

The resulting change in the vorticities are as given in Figs. 10 and 11. As can be seen from these results, the wall singularity at the stagnation point further diffuses inward for this particular grid.

Another important point to be mentioned here is the solution of the second-order form of the convection equations, as stated in Eqs. (27) and (28). If one considers a regular finite element grid as shown in Fig. 12 and formulates the difference operator for a grid point (i,j), where the flowfield shows a one-dimensional change in the flowfield from (u_1,v_1) to (u_2,v_2), it can be shown that the linearized differential equation ($\rho=$ const) to be solved becomes

$$(u_1^2+u_2^2)\alpha_{,xx}+(v_1^2+v_2^2)\alpha_{,yy}+2(u_1v_1+u_2v_2)\alpha_{,xy}=0 \quad (48)$$

This differential equation is parabolic only when $u_1=u_2$ and $v_1=v_2$; otherwise it is always an elliptic equation. It is therefore expected that any sharp changes in the direction of the streamline will introduce diffusion across the streamline.

Another test was performed on the original grid in Fig. 1. To show the effect of the trailing-edge singularity, the grid resolution was increased near the wall by placing an additional row of elements closer to the wall as shown in Fig. 9c. The obtained numerical results are as shown in Figs. 13 and 14. As can be seen from these results, the surface singularity is further restricted to the boundary streamline; yet, the disturbance still propagates along the surface streamline. It is important to note again that such a singularity occurs only in the calculation of vorticities from the derivatives of α and β. However, for the computation of velocities and densities, the same derivatives of these variables are necessary which indicate the necessity of second-order accuracy in both α and β terms for accurate solution of rotational flows.

Finally, no noticeable differences in the velocity and pressure distributions were observed in all three grids, this is

Table 1 Converged exit flow conditions using two different boundary conditions

α		Mach No.		p/p_∞		$\Delta p_T{}^a \times 10^3$	
I	II	I	II	I	II	I	II
0.0047	0.0047	0.6417	0.6429	0.9947	0.9937	0.3294	0.3302
0.0219	0.0220	0.6470	0.6481	0.9947	0.9937	0.2872	0.2881
0.0529	0.0530	0.6553	0.6564	0.9946	0.0036	0.2206	0.2213
0.0962	0.0963	0.6644	0.6656	0.9945	0.9934	0.1457	0.1463
0.1524	0.1525	0.6727	0.6741	0.9943	0.9931	0.0763	0.0767
0.2221	0.2223	0.6789	0.6802	0.9941	0.9929	0.0259	0.0261
0.3055	0.3058	0.6819	0.6830	0.9938	0.9928	0.0025	0.0025
0.4024	0.4027	0.6829	0.6836	0.9931	0.9925	0.0000	0.0000
0.5124	0.5128	0.6837	0.6838	0.9924	0.9923	0.0000	0.0000
0.6357	0.6360	0.6847	0.6841	0.9915	0.9921	0.0000	0.0000
0.7722	0.7725	0.6856	0.6843	0.9908	0.9919	0.0000	0.0000
0.9219	0.9220	0.6861	0.6844	0.9904	0.9918	0.0000	0.0000

[a] $\Delta p_T =$ total pressure loss $= 1 - e^{-S/R}$.

attributed to the relatively low vorticities generated by the shock.

Boundary Conditions

The boundary conditions for the solution of Eqs. (26-28) are as specified by Eqs. (29) and (30). They require the specification of mass flux and the entropy flux at the boundaries. For a typical flow configuration sketched in Fig. 15, the flux conditions for mass are specified at the inlet and exit of the channel. The entropy flux generated at the shock is specified at the exit as a function of α. Also, the values of α and β are specified from isentropic flow conditions at the irrotational flow region. Thus, Dirichlet-type boundary conditions are imposed for α and β at the upstream boundary on the shock. Three sets of downstream boundary conditions were tested to check their effect on accuracy and convergence. These cases are:

Case I: Updating the flux terms of f_ϕ and f_α as calculated from the previous iteration step.

Case II: Updating the entropy flux term for f_α at each step, and calculating the mass flux by specifying the downstream pressures as $p_{+\infty}=p_{-\infty}$.

Case III: Updating the entropy flux term for f_α at each step while calculating the downstream mass flux by assuming the flow to be horizontal and integrating the existing vorticity distribution on the boundary to obtain the velocities.

In terms of convergence rate, these attempts did not exhibit any significant differences. The converged solutions for each case were close as indicated by the centroidal values in the exit elements given in Table 1.

VI. Concluding Remarks

The numerical scheme presented herein extends the applicability of widely employed relaxation schemes in computing potential flows for the solution of full Euler equations. As can be observed from the presented numerical results, one can use the potential solution as an initial approximation and calculate the Euler solution through a second set of iterations. Therefore, the basic computational tools previously developed for analyzing transonic potential flows, such as artificial viscosity in the supersonic pocket, shock capturing, shock fitting, etc., can be directly applied to the present scheme. The obtained results show that the rate of convergence of the Euler equations is basically governed by the rate of convergence of conservation of mass equation. This also suggests that efficient solution schemes developed for potential flows can be directly utilized with the present scheme. Considering that the steady potential flows can be calculated quite accurately and efficiently with relaxation schemes, one can expect similar performance from the solution of Euler equations through the present scheme. However, for stronger shocks with higher rotationality effects, the convergence of α and β equations may become more critical.

One of the significant features of the present scheme is the transformation of Euler equations into a set of second-order equations, coupled only through the local velocity vector. One can then solve these equations through a centered-difference formulation without resorting to any artificial viscosity, except in the supersonic pocket. As can further be seen from the numerical results, the solutions show no effects of diffusion while the vorticities are convected from the shock to the downstream. The iterative calculation of downstream boundary conditions (lagged one step in time), provides a simple and efficient procedure for determining the mass flux and vorticity conditions. The scheme can also be applied to external flow problems since the rotationality is defined at the boundaries as a function of the material coordinate α.

Finally, the formulation can be extended directly to three-dimensional flows. For general flows five variables are required. However, for the flow cases where the rotationality at the inlet is one-dimensional, only three variables (ϕ, α, and β) suffice. Such a three-dimensional application of the present method is forthcoming.

Acknowledgments

This research was sponsored by NASA Grant NSG-3294, Lewis Research Center, Cleveland, Ohio. The authors would like to thank R. V. Chima and P. M. Sockol for their valuable suggestions and encouragement. Support provided by the IUPUI Computing Services is gratefully acknowledged.

References

[1] Beam, R. M. and Warming, R. F., "An Implicit Finite-Difference Algorithm for Hyperbolic Systems in Conservation-Law Form," *Journal of Computational Physics*, Vol. 22, Sept. 1976, pp. 87-110.

[2] Ni, R. H., "A Multiple Grid Scheme for Solving Euler Equations," *Proceedings of AIAA Computational Fluid Dynamics Conference*, Palo Alto, Calif., June 1981, pp. 257-264.

[3] Jameson, A., Schmidt, W., and Turkel, E., "Numerical Solutions of Euler Equations by Finite Volume Methods Using Runge-Kutta Time Stepping Schemes," AIAA Paper 81-1259, Palo Alto, Calif., 1981.

[4] Steger, J. L. and Warming, R. F., "Flux Vector Splitting of the Inviscid Gasdynamic Equations with Application to Finite-Difference Methods," *Journal of Computational Physics*, Vol. 40, No. 2, 1981, pp. 263-293.

[5] Seliger, R. L. and Whitham, G. C., "Variational Principles in Continuum Mechanics," *Proceedings of Royal Society*, Ser. A, Vol. 305, 1968, pp. 1-25.

[6] Ecer, A. and Akay, H. U., "A Finite Element Formulation of Euler Equations for the Solution of Steady Transonic Flows," AIAA Paper 82-0062; also, *AIAA Journal*, Vol. 21, March 1983, pp. 343-350.

[7] Liepmann, H. W. and Roshko, A., *Elements of Gas Dynamics*, John Wiley, New York, 1957.

[8] Serrin, J., "Mathematical Principles of Classical Fluid Mechanics," *Handbuch Der Physik*, Vol. VIII/I, Springer Verlag, Berlin, 1959.

[9] Emmons, H. W., "The Numerical Solution of Compressible Fluid Flow Problems," NACA TN 932, May 1944.

[10] Hafez, M. and Lovell, D., "Numerical Solution of Transonic Stream Function Equation," *Proceedings of the AIAA Computational Fluid Dynamics Conference*, Palo Alto, Calif., June 1981, pp. 364-372.

[11] Ecer, A. and Akay, H. U., "Investigation of Transonic Flow in a Cascade Using the Finite Element Method," *AIAA Journal*, Vol. 19, Sept. 1981, pp. 1174-1182.

[12] v. Koppenfels, W., "Two Dimensional Potential Flow Past a Smooth Wall with Partly Constant Curvature," NACA TM 996, Nov. 1941.